

1 **Title: Synergetic impacts of turbulence and fishing reduce ocean biomass**

2

3 **Authors**

4 Jody C. McKerral<sup>1\*</sup>, Justin R. Seymour<sup>2</sup>, Trish J. Lavery<sup>1</sup>, Paul J. Rogers<sup>3</sup>, Thomas C. Jeffries<sup>4</sup>,  
5 James S. Paterson<sup>1</sup>, Ben Roudnew<sup>1</sup>, Charlie Huveneers<sup>1</sup>, Kelly Newton<sup>5</sup>, Virginie van Dongen-  
6 Vogels<sup>6</sup>, Nardi P. Cribb<sup>1</sup>, Karina M. Winn<sup>1</sup>, Renee J. Smith<sup>7,8</sup>, Crystal L. Beckmann<sup>3</sup>, Eloise  
7 Prime<sup>9</sup>, Claire M. Charlton<sup>10</sup>, Maria Kleshnina<sup>11</sup>, Susanna R. Grigson<sup>1</sup>, Marika Takeuchi<sup>12</sup>,  
8 Laurent Seuront<sup>13,14,15</sup>, James G. Mitchell<sup>1</sup>

9 **Affiliations**

10

11 <sup>1</sup>College of Science and Engineering, Flinders University, GPO Box 2100, Adelaide, SA 5000,  
12 Australia

13 <sup>2</sup>Plant Functional Biology and Climate Change Cluster, University of Technology Sydney,  
14 Sydney, NSW 2007, Australia

15 <sup>3</sup>Aquatic Sciences Centre, South Australian Research and Development Institute, Military Road,  
16 West Beach, SA 5024, Australia

17 <sup>4</sup>Medical Science, Western Sydney University, Locked Bag 1797, Penrith, NSW 2751, Australia

18 <sup>5</sup>SAWater, Adelaide, SA 5000, Australia

19 <sup>6</sup>Australian Institute of Marine Sciences, Townsville, QLD 4810, Australia

20 <sup>7</sup>College of Medicine and Public Health, Flinders University, GPO BOX 2100, Adelaide, SA  
21 5000, Australia

22 <sup>8</sup>South Australian Genomics Centre, South Australian Health and Medical Research Institute,  
23 Adelaide, SA 5000, Australia

24 <sup>9</sup>Port Macquarie Hastings Environmental Laboratory, 7 Major Innes Road, Port Macquarie,  
25 NSW 2444, Australia

26 <sup>10</sup>Centre for Marine Science & Technology, Curtin University, GPO Box U1987, Perth, WA  
27 6845, Australia

28 <sup>11</sup>Institute of Science & Technology Austria, Klosterneuburg Am Campus 1 3400 Austria

29 <sup>12</sup>National Oceanography Centre, Southampton, SO14 3ZH, United Kingdom

30 <sup>13</sup>CNRS, Univ. Lille, Univ. Littoral Côte d'Opale, UMR 8187, LOG, Laboratoire d'Océanologie  
31 et de Géosciences, F 62930 Wimereux, France

32 <sup>14</sup>Department of Marine Energy and Resource, Tokyo University of Marine Science and  
33 Technology, 4-5-7 Konan, Minato-ku, Tokyo 108-8477, Japan

34 <sup>15</sup>Department of Zoology and Entomology, Rhodes University, Grahamstown, 6140, South  
35 Africa.

36

37 **Acknowledgements:** Stephen J Hall, Peter G Strutton, Susan D Willmott, Xiaoke Hu, Song Sun,  
38 and Lisa Dann made helpful comments on early versions of the manuscript. This work was  
39 supported by Flinders University, CNRS and Australian Research Council grants to JGM, LS  
40 and JRS. Matthew D Russell, Shareena J White, Tomoyo Segawa and Rachel J Pillar helped with  
41 data collection.

42 **Funding:** This work was supported by Flinders University, CNRS and Australian Research  
43 Council grants to JGM, LS and JRS.

44 **Author contributions:** JGM, JCM, JRS & LS conceived the work

45 JCM, JGM & JRS wrote the paper

46 SRG, TJL, PJR, TCJ, JSP, BR, CH, KN, VvdV, NPC, KMW, RJS, CLB, EP, JRS and CMC  
47 gathered the data and helped with the analysis

48 JCM developed the model, gathered data, and did the analysis

49 MK contributed to model development

50 MT helped with analysis and contributed to writing, interpretation and insight

51 LS helped with analysis, and contributed to writing and interpretation and insight

52 **Competing interests:** the authors declare no conflicts of interest.

53 **Data and materials availability:** All data is available in the supplementary materials or online.

54 Code is available at <https://github.com/jcmckerral>.

55 **Abstract:**

56 A universal scaling relationship exists between organism abundance and body size<sup>1,2</sup>. Within  
57 ocean habitats this relationship deviates from that generally observed in terrestrial systems<sup>2-4</sup>,  
58 where marine macro-fauna display steeper size-abundance scaling than expected. This is  
59 indicative of a fundamental shift in food-web organization, yet a conclusive mechanism for this  
60 pattern has remained elusive. We demonstrate that while fishing has partially contributed to the  
61 reduced abundance of larger organisms, a larger effect comes from ocean turbulence: the  
62 energetic cost of movement within a turbulent environment induces additional biomass losses  
63 among the nekton. These results identify turbulence as a novel mechanism governing the marine  
64 size-abundance distribution, highlighting the complex interplay of biophysical forces that must  
65 be considered alongside anthropogenic impacts in processes governing marine ecosystems.

66

67 **Main Text**

68 Across all ecosystems, a fundamental scaling relationship exists between species abundance ( $A$ )  
69 and body size ( $W$ ), whereby:

$$70 \quad A \propto W^\alpha$$

71 and the exponent  $\alpha$  typically approximates  $-0.75^1$ . This universal rule derives from resource  
72 acquisition as a function of body size<sup>1</sup>, which is a barometer for ecosystem health that simplifies  
73 interactions in complex food webs and may direct fisheries management<sup>5</sup>. However, within  
74 marine ecosystems, the exponent for this relationship often differs from that in terrestrial  
75 ecosystems<sup>2</sup>. Life-history, trophic strategies, altered productivity, and fisheries are all proposed  
76 to alter the scaling slopes of both species size-abundance distributions and individual size  
77 spectra<sup>2-4,6</sup>. Here, we quantify, empirically and with an independent model, how fishing and  
78 ocean turbulence cause qualitatively distinct breaks in the global marine size-abundance  
79 distribution.

80  
81 For the scaling analysis we compiled size-abundance data for 2179 species, ranging from viruses  
82 to blue whales. Analyses were undertaken on a database built from primary literature and online  
83 databases ( $n = 15,146$  datapoints), with secondary verification undertaken using the manually  
84 curated literature data alone ( $n = 1719$ ) to ensure there was not systematic bias in the online  
85 sources (Methods); additionally, fits were undertaken through a balanced subsampling routine to  
86 ensure a diverse spread of species and sizes (Methods). As previously observed within individual  
87 size spectra<sup>3</sup>, nonlinearity was apparent in the log-transformed global size-abundance plot  
88 (Figure 1a). This coincided with a statistically verified break in the scaling value at the plankton-  
89 nekton transition of  $l \simeq 0.1$  m ( $l = 0.08$  m, 95% CI (0.06, 0.1)) (Methods). The marine virus to

90 marine invertebrate slope at  $\alpha = -0.77$  is comparable to terrestrial slopes<sup>7</sup>. However, for  
91 organisms  $\geq 0.1$  m  $\alpha$  was  $-1.9$  (Figure 1a, Table 1), representing a significant negative  
92 perturbation in the slope. A shift in biomass would only translate the line downward (i.e. change  
93 the intercept via a step break), but the large slope break evidenced by these two exponent values  
94 (Figure 1) is indicative of a more fundamental alteration in the mechanistic processes shaping the  
95 species size-abundance distribution and ecosystem structure.

96  
97

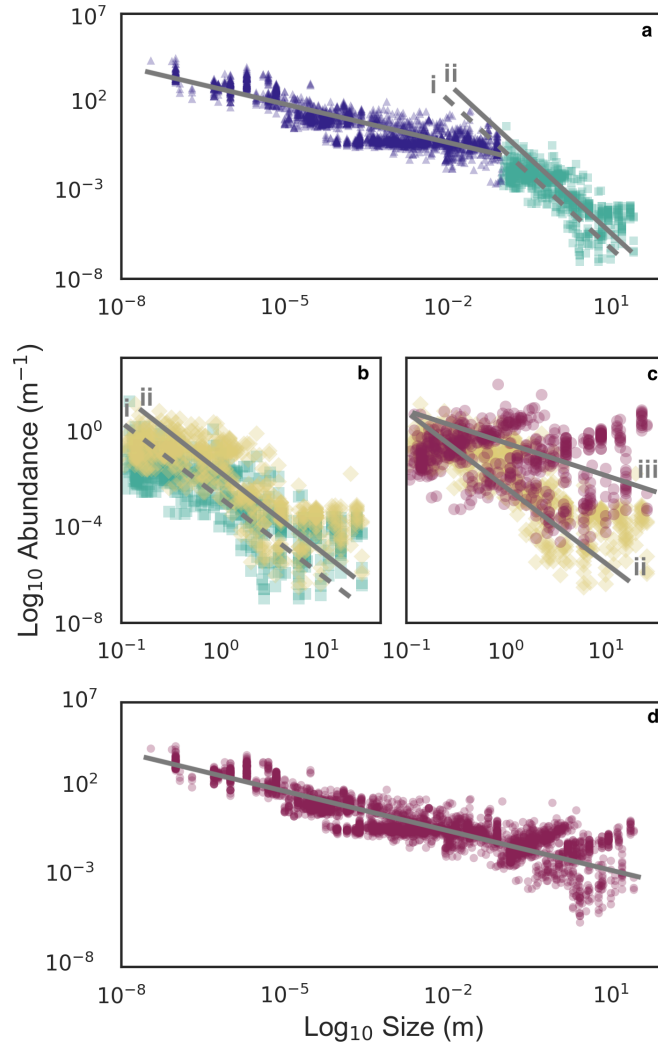
98

Data type	Manually curated dataset	Full dataset	Model
Laminar	-0.74 (-0.79, -0.69)	-0.77 (-0.81, -0.73)	-0.73 (-0.76, -0.71)
Turbulent (raw)	-2.5 (-2.7, -2.3)	-1.9 (-2.0, -1.8)	-
Turbulent (fishing adjusted)	-2.5 (-2.6, -2.2)	-1.7 (-1.8, -1.6)	-2.1 (-2.2, -2.0)
Turbulent (adjusted)	-0.94 (-1.1, -0.74)	-0.56 (-0.69, -0.43)	-
Full distribution (turbulence adjusted)	-0.83 (-0.88, -0.79)	-0.73 (-0.76, -0.69)	-0.71 (-0.72, -0.71)

99 **Table 1.** Estimates of the scaling exponent ( $\alpha$ ) with 95% confidence intervals for the empirical  
100 data (raw and adjusted) and the model simulated data, all calculated from 10,000 bootstrapped  
101 values (Methods).

102

103



104

105 **Figure 1: Empirical size-abundance distribution.** For consistency of units, here we use length

106 scales rather than mass/density; it is to be noted that as the transformation of both axes is the

107 same, the relationship between size and abundance remains unchanged (Methods). **(a)** Size

108 versus abundance for viruses to blue whales. There is a break in the scaling relationship at 0.1m.

109 Blue triangles represent plankton ranging from viruses to zooplankton and invertebrates. Green

110 squares are fished nekton, ranging from small fish to whales. Line (i) is the best fit to the scaling

111 of nekton. **(b)** Line (ii) is corrected abundance for removal by fishing, with yellow diamonds

112 showing the fishing-corrected values. **(c)** Line (iii) corrects for extra foraging due to turbulent

113 dispersion, shown by red circles. (i) to (ii) is predominantly a vertical translation and (ii) to (iii)  
114 is a slope correction. After both corrections all points fall along a line with a slope of  $-0.73$  **(d)**.

115  
116 To find the cause of the break in the marine size-abundance relationship, we note that fishing has  
117 reduced the abundance of fish, pinnipeds, sea turtles and marine mammals by up to 99%<sup>8</sup>. We  
118 corrected for this by adjusting the abundances of impacted populations to pre-human impact  
119 estimates<sup>8</sup>. This caused a significant ( $p < 0.01$ ) upward translation of the scaling line, removing  
120 the step break in the dataset and corroborating earlier findings<sup>5</sup>. However, whilst the translation  
121 is indicative of a decreased abundance of animals larger than 0.1 m, correcting for fishing did not  
122 result in a change in exponent, rather just a vertical shift in the data (Figure 1b, Table 1). The  
123 size-abundance distribution may be interpreted as an average or upper bound on local population  
124 densities<sup>2</sup>. The slope change is thus indicative of a constraint limiting nekton abundances which  
125 is not present in planktonic or terrestrial systems. To probe for a mechanistic explanation of the  
126 exponent change, we note that many aquatic organism scaling laws break at  $\approx 0.1$  m<sup>6,9,10</sup>; this  
127 size corresponds to the laminar-turbulent transition, where the change in the physical fluid  
128 environment causally affects the biology<sup>6,10</sup>. We subsequently tested the hypothesis that the  
129 change in scaling value is due to implicit and explicit costs associated with turbulence: that is,  
130 nekton must expend energy actively moving to match planktonic prey distributions, and that this  
131 expenditure propagates through higher trophic levels.

132  
133 Aquatic predators and grazers are challenged by the chaotic nature of turbulence. As absolute  
134 abundances of resources scale similarly in three-dimensional aquatic and two-dimensional  
135 terrestrial environments<sup>11</sup>, their statistical distribution is scarcer in the three-dimensional ocean.

136 Plankton live within patches created by an interplay of physical and biological processes<sup>12</sup>.  
137 Within these resource hotspots, plankton foraging and movement is localised and constrained  
138 within the patch, allowing them to use hunting strategies such as chemotaxis or rheotaxis to  
139 maximise their food acquisition<sup>13,14</sup>; that is, plankton move passively with the turbulence that  
140 creates the aggregations. Beyond several millimetres and up to ten centimetres is a transition  
141 zone where eddies play an increasingly important role. Whilst they are below the swimming  
142 speeds of most fish, eddies on the scale of tens to hundreds of metres cause bulk transport and  
143 dispersal. Mesoscale eddies reach hundreds of kilometres in diameter and can move organisms  
144 hundreds or thousands of kilometres<sup>15</sup>. Food may not be transported, or it may be consumed and  
145 not replaced due to low light, low temperature or other unfavourable conditions<sup>16</sup>. Thus, nekton  
146 must migrate between patches to feed, which are continually and unpredictably dispersed,  
147 meaning they have resource encounter rates that typically cannot be bettered using local  
148 information<sup>17</sup>. Nekton live at a scale where the foraging landscape is highly fragmented and  
149 disordered due to these physical processes, and operate on biological timescales which are  
150 significantly longer than eddy lifespans<sup>16,18</sup>. As they are trophically linked to the plankton, they  
151 must actively work to overcome the dispersal, ultimately increasing their locomotory costs,  
152 which also grow with prey size<sup>19</sup>. Short distance dispersal within or just beyond local habitats is  
153 difficult to quantify. However, at a global scale, physical dispersal – and consequently the spatial  
154 distribution of plankton – follows the Kolmogorov power law for the turbulent energy cascade<sup>12</sup>.  
155 The overall effect is that dispersal, encoded here as the separation distance, is a key factor in  
156 nekton survival. We propose that resource acquisition forces nekton movement to follow the  
157 turbulence-driven distribution of plankton, increasing energy expenditure<sup>20</sup>, and consequently  
158 reducing available energy for growth and reproduction, which decreases abundances. The



159 positioning of the break in the scaling relationship at the laminar-turbulent transition is consistent  
160 with this reasoning. Testing the hypothesis that turbulence increased the nekton slope by  
161 adjusting for the Kolmogorov power law, which affected small fish the least and large pelagics  
162 the most, removed the structural break in the distribution and resulted in a near-canonical  
163 exponent of  $\alpha = -0.73$  for the entire distribution (Figure 1d, Table 1).

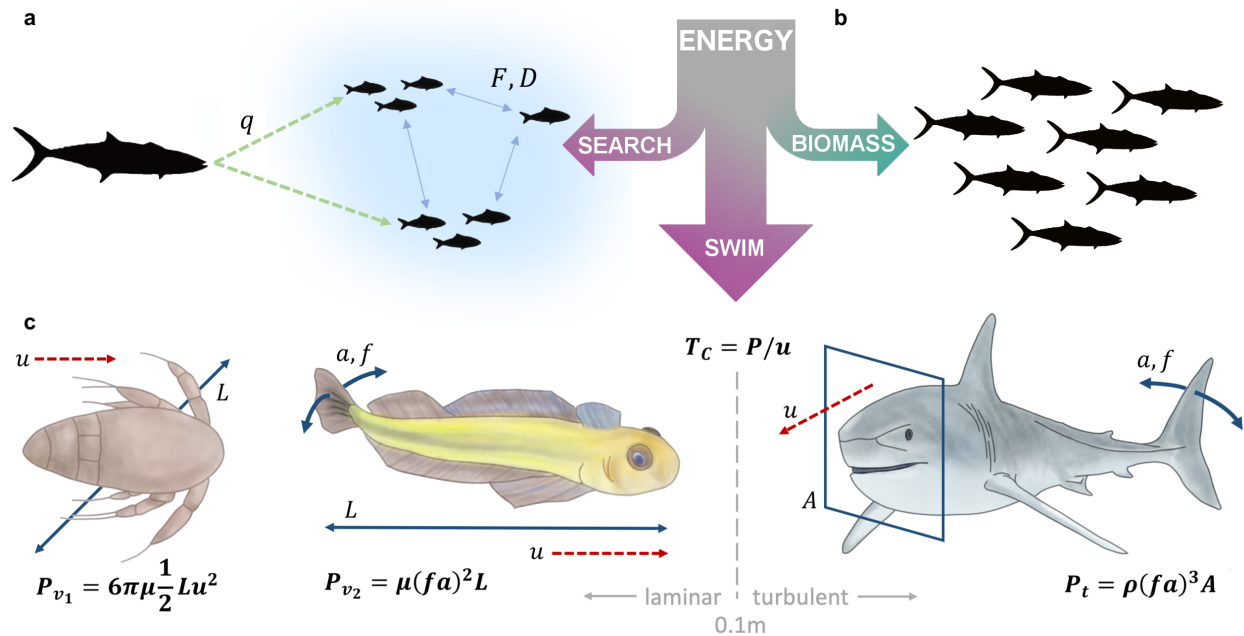
164  
165 To build a minimal model which captures this phenomenon, we note other scaling breaks for  
166 aquatic organisms<sup>6</sup> also occur at 0.1 m due to movement changes at the laminar-turbulent  
167 transition<sup>10</sup>. The classical assumption that swimming is more energetically efficient than  
168 running<sup>21</sup> does not consider drag, which increases with the square of velocity and carries extreme  
169 metabolic cost<sup>22,23</sup>. Research examining cost of swimming may also underestimate real-world  
170 metabolic effort for nekton as it frequently uses theoretically ‘optimal’ size-speed scaling<sup>9</sup> rather  
171 than utilising empirical values which are steeper<sup>6</sup>. Finally, relative consumption rates are higher  
172 in oceanic than terrestrial environments, yet a steeper inverse scaling of nekton abundances in  
173 marine systems exists even at high resource densities<sup>11</sup>. This discrepancy has not been resolved  
174 but indicates there must be a significant energetic cost associated with living and feeding in  
175 oceanic environments that has not been considered. We incorporated classical formulations of  
176 swimming cost for organisms living in laminar and turbulent environments, together with  
177 foraging effort, into a size-dependent predator-prey model to assess these effects (Figure 2). In  
178 short, we expand the trophic transfer efficiency parameter,  $\varepsilon$ , in the classical Rosenzweig-  
179 MacArthur predator-prey model to account for energy diversion toward locomotion (Equation 1).  
180 In this equation, each parameter scales according to the length  $l$  of the organism (m), allowing it  
181 to be solved across the full size range.

$$\begin{aligned}\frac{\partial x}{dt} &= rx \left(1 - \frac{x}{K}\right) - \frac{\varphi xy}{h + x} \\ \frac{\partial y}{dt} &= \frac{\varepsilon \varphi xy}{h + x} - \delta y\end{aligned}\tag{1}$$

182 Capturing the shift in movement energy budgets from the laminar to the turbulent regime is  
183 achieved by using the relation  $\varepsilon \propto l^{-c-q(F-D)}$  (24). The exponent  $c$  accounts for the scaling of  
184 swimming cost relative to basal metabolic rate, and the term  $q(F - D)$  depicts resource search  
185 effort (Figure 2) (refer to Methods for the complete derivation).  
186  
187 Including locomotion cost for simulated predator-prey combinations from primary producers to  
188 blue whales reproduced the empirical results. Calculating the slope for model equilibria  
189 abundances in the turbulent regime resulted in a value of  $-2.1$ , consistent with the data (Figure  
190 3a, Table 1). For the laminar model, and the turbulence-corrected predator-prey formulation  
191 across the entire data set, the slopes were  $-0.77$  and  $-0.73$  respectively, matching the empirical  
192 results (Figure 3b, Table 1). In our model, living in a turbulent fluid regime impacts the system  
193 by translating the predator abundances downward. This means prey support fewer predators in a  
194 turbulent environment than they would in viscous or terrestrial regimes because of the increased  
195 energetic costs of foraging in turbulence. Increasing locomotion energy budgets decreases  
196 biomass transfer to higher trophic levels where reduced prey availability places even more  
197 restrictions on energetic resources<sup>19</sup>, pushing large marine organism abundances closer to an  
198 unviable population threshold where natural population fluctuations also render them more  
199 vulnerable to extinction<sup>25</sup>.

200

201



202

203 **Figure 2: Energy partitioning - organisms have a finite energy budget which is split**

204 **between movement and creation of new biomass. (a)** A search effort term  $q(F - D)$  is

205 described by the scaling of swimming speed ( $q$ ), as well as parameters  $F$  and  $D$ , which denote

206 resources' fractal dimension (space-filling amount) and the physical dimension of the search

207 space respectively. **(b)** Energy not spent on locomotion is utilised in reproduction and creation of

208 new biomass. **(c)** Transport/swim cost ( $T_C$ ) is defined as power,  $P$ , divided by speed  $u$ . In the

209 laminar regime, power for viscous paddlers, such as copepods, is described by length (diameter)

210  $l$ , speed, and viscosity  $\mu$ . Viscous undulatory swimmer power (i.e. larvae or small fish) is given

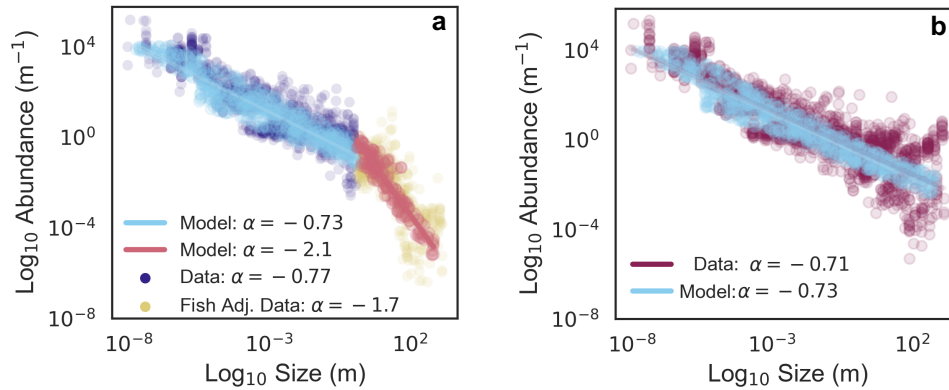
211 by kick frequency  $f$ , kick amplitude  $a$ , length, and viscosity  $\mu$ . In the turbulent regime power is

212 described by kick frequency and amplitude, frontal area  $A$  and fluid density  $\rho$ . We use these

213 formulae to calculate size scaling exponents for swimming cost. The values can then be used in

214 the master equation (Equation 1) to capture changes in energy partitioning across the size range.

215



216

217 **Figure 3:** Rosenzweig-MacArthur model results. **(a)** Plankton (dark blue) with fishing corrected  
218 empirical data (yellow), the laminar model simulated data ( $l < 0.1$  m, pale blue) and turbulent  
219 model simulated data ( $l \geq 0.1$  m, red). **(b)** Fishing and turbulence corrected data (purple  
220 circles), are shown with the model simulated data (pale blue) superimposed over the data-fitted  
221 regression line.

222

223 As our model includes a parameter for resource density, direct impacts of overfishing may also  
224 be incorporated. We find that whilst heavy fishing could theoretically perturb the size-abundance  
225 scaling value by decreasing resource saturation  $F$ , the search effort multiplier  $q$  is  
226  $\sim 0.17$  (relative to mass). This means it is a slow parameter, which also reaches an asymptotic  
227 value as  $F \rightarrow 0$ . Hence, whilst fishing removes biomass, our integrated model indicates it could  
228 only perturb the size-abundance scaling law by  $\approx -0.2$  before the asymptote is reached. This is  
229 an order of magnitude less impact than turbulence effects, and entirely consistent with what we  
230 observe with our data (Table 1).

231

232 A complicating factor with our analysis is that organisms and biomes are not fixed physical or  
233 chemical variables. Their characteristics can change in response to environmental pressures.  
234 Ecosystem-wide size shifts in size-abundance relationships may be exacerbated by compensatory  
235 genetic changes, particularly when they have occurred under strong selection pressures such as  
236 fishing. Such a fisheries-induced evolution (FIE) causes further size reduction and earlier  
237 maturation age<sup>26</sup>, which could alter the scaling relationship. To assess the relative impact of FIE,  
238 we extracted data from 113 time series for 10 commercially exploited species of fish, and  
239 assessed global changes in size and age at maturation. There was a mean decline of 11% in size  
240 or age at maturity, when accounting for gender, species, and length of study (Methods). The  
241 results from 10 of the 14 studies led to the conclusion that these changes were attributable to  
242 fishing pressure<sup>26</sup>. In considering FIE's contribution to universal size-abundance scaling, the  
243 breadth and size of our dataset gives insight into the signal-to-noise ratio for this problem. It  
244 would be extremely challenging to detect shifts in a global scaling law over the restricted size  
245 range of 0.1 to 2 m used for FIE impacts. While prior research suggests that FIE can perturb  
246 local scaling properties<sup>27</sup>, we argue an 11% impact (or even significantly greater) would not be  
247 enough to shift the global size-abundance scaling value of nekton by  $-1$  or more. We conclude  
248 that scaling alterations occurring due to FIE would be small relative to the turbulence effect  
249 explored in this paper.

250

251 Global size-abundance laws provide a different form of ecological insight to that given by local  
252 scaling behaviour, as they capture macroscale, aggregate processes rather than examining small-  
253 scale drivers such as inter- and intra-specific trait variation<sup>2</sup>. In this context, we introduce  
254 turbulence, and its impact on energy and movement cost for large organisms, as a novel but

255 important process to consider for ocean ecosystems. Climate change impacts have the potential  
256 to exacerbate these costs, as current and predicted increases in ocean surface energy<sup>28</sup> will  
257 increase nekton foraging and locomotion costs<sup>29</sup>, whilst warming temperatures increase  
258 respiration rates, reduce global primary productivity<sup>30</sup>, and cause greater resource patchiness<sup>31</sup>,  
259 forcing increased movement cost. Turbulence may thus reduce the capacity of nekton to  
260 withstand fishing pressure as we begin to observe oceanic anthropogenic impacts classically  
261 associated with terrestrial systems, including loss of large apex predators, shifts to smaller size,  
262 and a faster onset of sexual maturity. We propose that a deeper understanding of the role  
263 physical mechanistic processes play in structuring marine ecosystems will be necessary when  
264 formulating strategies to preserve biodiversity and retain the productivity of ocean resources in  
265 future.

266

267 **References**

- 268
- 269
- 270 1 West, G. B. & Brown, J. H. The origin of allometric scaling laws in biology from  
271 genomes to ecosystems: towards a quantitative unifying theory of biological structure and  
272 organization. *Journal of experimental biology* **208**, 1575-1592 (2005).
- 273 2 White, E. P., Ernest, S. K. M., Kerkhoff, A. J. & Enquist, B. J. Relationships between  
274 body size and abundance in ecology. *Trends in ecology & evolution* **22**, 323-330 (2007).
- 275 3 Blanchard, J. L., Heneghan, R. F., Everett, J. D., Trebilco, R. & Richardson, A. J. From  
276 bacteria to whales: using functional size spectra to model marine ecosystems. *Trends in  
277 ecology & evolution* **32**, 174-186 (2017).
- 278 4 Graham, N. A. J., Dulvy, N. K., Jennings, S. & Polunin, N. V. C. Size-spectra as  
279 indicators of the effects of fishing on coral reef fish assemblages. *Coral Reefs* **24**, 118-  
280 124 (2005).
- 281 5 Garcia, S. M. *et al.* Reconsidering the consequences of selective fisheries. *Science* **335**,  
282 1045-1047 (2012).
- 283 6 Andersen, K. H. *et al.* Characteristic sizes of life in the oceans, from bacteria to whales.  
284 *Annual Review of marine science* **8**, 217-241 (2016).
- 285 7 Damuth, J. Population density and body size in mammals. *Nature* **290**, 699-700 (1981).
- 286 8 Lotze, H. K. & Worm, B. Historical baselines for large marine animals. *Trends in  
287 ecology & evolution* **24**, 254-262 (2009).
- 288 9 Bale, R., Hao, M., Bhalla, A. P. S. & Patankar, N. A. Energy efficiency and allometry of  
289 movement of swimming and flying animals. *Proceedings of the National Academy of  
290 Sciences* **111**, 7517-7521 (2014).
- 291 10 Gazzola, M., Argentina, M. & Mahadevan, L. Scaling macroscopic aquatic locomotion.  
292 *Nature Physics* **10**, 758 (2014).
- 293 11 Pawar, S., Dell, A. I. & Savage, V. M. Dimensionality of consumer search space drives  
294 trophic interaction strengths. *Nature* **486**, 485-489 (2012).
- 295 12 Strutton, P. G., Mitchell, J. G., Parslow, J. S. & Greene, R. M. Phytoplankton patchiness:  
296 quantifying the biological contribution using fast repetition rate fluorometry. *Journal of  
297 Plankton Research* **19**, 1265-1274 (1997).
- 298 13 Smriga, S., Fernandez, V. I., Mitchell, J. G. & Stocker, R. Chemotaxis toward  
299 phytoplankton drives organic matter partitioning among marine bacteria. *Proceedings of  
300 the National Academy of Sciences* **113**, 1576-1581 (2016).
- 301 14 Jiang, H. & Kiørboe, T. The fluid dynamics of swimming by jumping in copepods.  
302 *Journal of the Royal Society Interface* **8**, 1090-1103 (2011).
- 303 15 Lehahn, Y., d'Ovidio, F., Lévy, M., Amitai, Y. & Heifetz, E. Long range transport of a  
304 quasi isolated chlorophyll patch by an Agulhas ring. *Geophysical Research Letters* **38**  
305 (2011).
- 306 16 Condie, S. & Condie, R. Retention of plankton within ocean eddies. *Global Ecology and  
307 Biogeography* **25**, 1264-1277 (2016).
- 308 17 Sims, D. W. *et al.* Scaling laws of marine predator search behaviour. *Nature* **451**, 1098  
309 (2008).
- 310 18 Vortmeyer-Kley, R., Lünsmann, B., Berthold, M., Gräwe, U. & Feudel, U. Eddies: fluid  
311 dynamical niches or transporters?-A case study in the Western Baltic Sea. *Frontiers in  
312 Marine Science* **6**, 118 (2019).

- 313 19 Goldbogen, J. *et al.* Why whales are big but not bigger: Physiological drivers and  
314 ecological limits in the age of ocean giants. *Science* **366**, 1367-1372 (2019).
- 315 20 Speers-Roesch, B., Norin, T. & Driedzic, W. R. The benefit of being still: energy savings  
316 during winter dormancy in fish come from inactivity and the cold, not from metabolic  
317 rate depression. *Proc. R. Soc. B* **285**, 20181593 (2018).
- 318 21 Schmidt-Nielsen, K. *Scaling: why is animal size so important?* , (Cambridge University  
319 Press, 1984).
- 320 22 Bejan, A. & Marden, J. H. Unifying constructal theory for scale effects in running,  
321 swimming and flying. *Journal of Experimental Biology* **209**, 238-248 (2006).
- 322 23 Goldbogen, J. A. *et al.* Scaling of lunge-feeding performance in rorqual whales: mass-  
323 specific energy expenditure increases with body size and progressively limits diving  
324 capacity. *Functional Ecology* **26**, 216-226 (2012).
- 325 24 Nilsen, E. B., Finstad, A. G., Næsje, T. F. & Sverdrup-Thygeson, A. Using mass scaling  
326 of movement cost and resource encounter rate to predict animal body size–population  
327 density relationships. *Theoretical population biology* **86**, 23-28 (2013).
- 328 25 Olden, J. D., Hogan, Z. S. & Zanden, M. Small fish, big fish, red fish, blue fish: size-  
329 biased extinction risk of the world's freshwater and marine fishes. *Global Ecology and*  
330 *Biogeography* **16**, 694-701 (2007).
- 331 26 Heino, M., Díaz Pauli, B. & Dieckmann, U. Fisheries-induced evolution. *Annual Review*  
332 *of Ecology, Evolution, and Systematics* **46**, 461-480 (2015).
- 333 27 Jennings, S. & Blanchard, J. L. Fish abundance with no fishing: predictions based on  
334 macroecological theory. *Journal of Animal Ecology* **73**, 632-642 (2004).
- 335 28 Bhatia, K., Vecchi, G., Murakami, H., Underwood, S. & Kossin, J. Projected Response of  
336 Tropical Cyclone Intensity and Intensification in a Global Climate Model. *Journal of*  
337 *Climate* (2018).
- 338 29 Silva, A. T., Katopodis, C., Santos, J. M., Ferreira, M. T. & Pinheiro, A. N. Cyprinid  
339 swimming behaviour in response to turbulent flow. *Ecological Engineering* **44**, 314-328  
340 (2012).
- 341 30 Cabré, A., Marinov, I. & Leung, S. Consistent global responses of marine ecosystems to  
342 future climate change across the IPCC AR5 earth system models. *Climate dynamics* **45**,  
343 1253-1280 (2015).
- 344 31 McHenry, J., Welch, H., Lester, S. E. & Saba, V. Projecting marine species range shifts  
345 from only temperature can mask climate vulnerability. *Global change biology* (2019).  
346



347

## 348 **Methods**

349 The reader may refer to Extended Data, Table S4 for symbol definitions used throughout the  
350 Methods. All statistical testing was conducted in MATLAB R2019b (Mathworks), and code is  
351 available at <https://github.com/jcmckerral>.

## 352 **Data**

### 353 *Data sourcing and aggregation*

354 To assess the size-abundance scaling relationship, we examined data for over 2100 species,  
355 encompassing over 800 genera (bacteria/viruses excluded from diversity counts) (Extended Data,  
356 Table S1, S7). For quality purposes, we undertook analysis with two datasets. The first was  
357 manually curated from over 200 articles to ensure there was not systematic bias within database  
358 sources, and consists of 1719 size-abundance pairs across 700+ species (Extended Data, Table  
359 S1). The second dataset expands on the first via the inclusion of a further 13,455 entries  
360 predominantly sourced from online databases, for a total of 15,174 data points (Extended Data,  
361 Table S7). Five databases were used: IMOS (flow cytometry and zooplankton)<sup>32,33</sup>, Tara Oceans  
362 (flow cytometry)<sup>34</sup>, Phytobase<sup>35</sup> for phytoplankton, a global diatom database<sup>36</sup>, and a reef fish  
363 dataset<sup>37</sup>. Size data was taken from the same source as the abundance data, or if it was not  
364 included, we assigned the average adult size for that taxon referenced from WoRMS<sup>38</sup>,  
365 fishbase<sup>39</sup>, or (36) for diatoms. All database entries which dated pre-2000 were removed to  
366 reduce the chance of methodological/quality control problems being introduced from older data.  
367 For Phytobase entries, any data with the flags ‘unrealistic day or year’ and ‘presumably  
368 sedimentary’ were deleted; we note this particular database is otherwise well suited to this

369 application as capturing local diversity patterns is not critical for global size density analyses<sup>2</sup>.  
370 For the flow cytometry data, any entries which had not undergone or passed quality control  
371 checks were removed.  
372  
373 Next, we outline pooling information for taxonomic/sampling groups. For most nekton,  
374 abundance estimates were given at the species level, with the exception of hard-to-differentiate  
375 taxa, e.g. striped/common dolphins. Unless the data had been provided that way by the primary  
376 source, no averaging or grouping was undertaken. For bacterial and viral abundances, we elected  
377 to use flow cytometric data rather than DNA-based methods, as the high variance in copy  
378 numbers of marker genes in prokaryotes precludes reliable estimates. (Note that size  
379 measurements for bacteria and viruses were given by microscopy-based sources, not flow  
380 cytometry.) In addition, defining ‘species’ grouping is inherently problematic for microbes. No  
381 manually curated data was aggregated unless that was its original format. For the databases, we  
382 pooled according to the following principles. Firstly, we took taxa abundance averages by year  
383 and location. A single location was taken to be one station, or the same degree of  
384 latitude/longitude. We averaged at the lowest available taxonomic level (usually genus for  
385 organisms <5E-4m, and species for anything larger), and selected taxa which, together, provided  
386 >90% of the total abundance of that sample to avoid skewing with singletons; this also aligns  
387 with the principle of size-abundance distributions often being representative of abundance  
388 average or upper bounds<sup>2</sup>. The exceptions to this pooling rule were for targeted flow cytometry  
389 counts of abundant cyanobacteria (*Prochlorococcus*, *Synechococcus*), which we included as is.  
390

391 Abundance data is localised, hence spatial and temporal variation across local snapshots captures  
392 natural variability of populations across space and time. Therefore, the inclusion of data from  
393 different environments, e.g. tropical/temperate, or low/high biomass regions, or across different  
394 sampling efforts, is suitable – and even desirable – as the goal is to build the universal  
395 distribution, which should ideally contain a broad spread of data<sup>2</sup>. Given the similarity between  
396 the manually curated and complete database results, and the generally well-behaved nature of the  
397 model statistics (Figures S1-S3), we elected not to transform or apply other corrections to the  
398 data. We acknowledge there is certainly variance introduced from species trait differences, and  
399 potentially from inconsistencies from underlying experimental methods. However, these impacts  
400 would remain with noise factor of this dataset. Furthermore, whilst more targeted studies can be  
401 sensitive to this variance due to scaling size range and data limitations (e.g. bony fish, at ~3  
402 orders of mass magnitude)<sup>2</sup>, fitting the scaling exponent over 23 orders magnitude, with this  
403 quantity of aggregated data, drastically mitigates the effect of any one source of error. Notably,  
404 the noise was sufficiently low for a strong statistical signal without the need for any  
405 manipulation, which could introduce other errors or biases, and reduce transparency of the result.

#### 406 *Standardisation and units*

407 Due to the large mass range (> 23 orders of magnitude), measuring uncertainty in the body mass  
408 of microorganisms<sup>40</sup>, and to ensure units were consistent in downstream analyses, we used body  
409 length,  $l$  (m), as the measure of organism size. To accurately compare data sets where abundance  
410 measurements were presented either as species numbers per unit volume or per unit area, and to  
411 account for organism behaviour, we calculated the separation distance,  $d$  (m), between  
412 organisms as a proxy measurement for abundance. To calculate separation distances, it was  
413 assumed the spatial distribution of organisms followed a Poisson distribution. Thus, the

414 separation distance for organisms where abundance was measured per unit area was given by  
415  $d = C^{-1/2}$ , and per unit volume,  $d = C^{-1/3}$ . Under the assumption that organism mass is  
416 approximately proportional to organism volume, the transformation of both axes in the size-  
417 abundance plot is the same. Therefore, our standardisation to length does not change the  
418 empirical scaling values, nor does it disproportionately impact one part of the distribution, but  
419 instead ensures consistency with units in the physics-based processes and derivations used in the  
420 analyses. We acknowledge that organism mass and length generally do not have a perfect cube  
421 root relationship. However, this is a standard transformation utilised when investigating  
422 bioenergetics of swimming organisms<sup>9</sup>; we also note that any deviation from a cube root  
423 relationship would be applicable across the full distribution and therefore not change the key  
424 outcomes of our analysis relating to the structural break.

425

426 We now discuss the raw data and the potential errors that may have arisen due to this  
427 standardisation. Plankton data was near universally presented by volume; we note that plankton  
428 distributions are by definition patchy and this variance far exceeds that of methodological error.  
429 Volume-based measurements in the reef fish dataset were based on study areas <30m deep and  
430 already undergone significant quality controls for accuracy; we did not undertake any further  
431 corrections. We assumed volume-based data for small nekton in the manually curated literature  
432 data did not require further adjustments. We acknowledge some small amount of error may have  
433 been introduced under this assumption in the event that depths were incorrectly measured, but  
434 note that (a) in the context of incorrectly measured depths, the cube root transformation reduces  
435 the impact of that error and (b) the data covers approximately 0.5 of an order of (length)  
436 magnitude, meaning that impacts on the full distribution would be minimal, particularly after

437 log-transformation. For marine megafauna, only studies using standard methodologies according  
438 to transect/aerial surveys were included. It is to be noted that most of the length- or area-based  
439 abundance measurements in the dataset were aerial survey data of marine mammals, and not of  
440 benthic organisms.

#### 441 *Power law model fitting methods*

442 To determine the scaling relationship across the dataset, organism length was plotted against the  
443 inverse of the separation distance  $1/d$  ( $\text{m}^{-1}$ ) on a logarithmic scale, so that  $d \propto l^{-\tau}$ , where  $\tau$  is a  
444 scaling exponent. Note that we consider a global, bivariate, size-abundance distribution more  
445 commonly applied in terrestrial settings, and not the univariate size distribution often studied in  
446 aquatic environments<sup>2</sup>. As the data is bivariate, the methods developed for univariate distribution  
447 fits are not directly applicable<sup>41</sup>. Regression methods are standard for the bivariate case, and may  
448 be used provided the dependent variable contains higher measurement error than the independent  
449 variable<sup>42</sup>. Therefore, following a residuals analysis, the models for plankton and nekton were  
450 fitted using ordinary least squares on the log-transformed data (residuals plots provided in  
451 Figures S1-S2). For the fits, a balanced subsampling routine was used to ensure an even spread  
452 of data across the distribution and improve fit quality<sup>43</sup>. We did not use a naive with-replacement  
453 bootstrapping routine as this would simply bias the sampling towards whichever data (taxa  
454 and/or sizes) were most frequent in our database. Furthermore, as large databases typically had  
455 large groups of data clustered together (e.g. Figure 1a, where various clumps of data may be  
456 observed), subsampling mitigated against one database, taxon, or size class dominating the fit.  
457 The data was stratified by organism sizes, and by taxa. We then randomly sampled  $m$  data points  
458 (without replacement) such that the quantity of data per (log)bin was uniform across the full size  
459 range and balanced the probabilities of sampling from different taxonomic groups. The optimal

460 subsampling size  $m$  is denoted by  $m = kn^\kappa$ , where  $n$  is the size of the dataset being drawn from,  
461  $k = 3$ , and  $\kappa = 0.5$  (43, 44). We then generated 10,000 parameter estimates for each model,  
462 where each estimate was created from subsampled data, for the laminar regime  $l < 0.1$ , turbulent  
463 regime  $l \geq 0.1$ , or complete size range. Percentile confidence intervals (95%) were created from  
464 the bootstrapped statistics. Representative linear model statistics are available in Tables S5-S6,  
465 and bootstrap histograms in Figure S3. For the  $\alpha$ -estimates from the Rosenzweig-MacArthur  
466 simulated data, we randomly generated  $m$  datapoints (matching the empirical subsample sizes)  
467 for the laminar, turbulent, and full size ranges. Confidence intervals were generated from fitted  
468 linear models on 10,000 model runs for each  $\alpha$ -estimate.

469  
470 *Structural break*

471 We used MATLAB's `fminbnd` function to find the segmented regression breakpoint which  
472 minimised MSE. This was bootstrapped for a percentile-based confidence interval on log-  
473 transformed, subsampled data (sampling method as for regressions).

474  
475 **Correction for Fishing**

476 To investigate the impact of fishing on the observed scaling relationships, organisms were  
477 assigned to groups of impacted large marine animals according to standard conventions<sup>8</sup>. These  
478 included organisms such as fish, sharks, pinnipeds, whales, sea turtles and sea birds. Separation  
479 distances were corrected for each group to reflect theoretical historical abundance values,  
480 assuming losses ranging between 50 and 99.7%<sup>8,45</sup>. Where no specific loss estimate was  
481 available, the mean decline for all large marine species (89%) was allocated<sup>8</sup>.

482  
483  
484

## 485 **Correction for Aquatic Turbulence**

486 The influence of aquatic turbulence on the scaling relationship for nekton was addressed by  
487 applying a phenomenological correction for the  $-5/3$  relationship arising from the Kolmogorov  
488 power-law of the inertial subrange of the energy spectrum<sup>46</sup>. The spectral energy density, a proxy  
489 of the variance of the variable under consideration, i.e. turbulent velocity fluctuations in the  
490 framework of fully developed turbulence, is given by  $E(k) = C_k \varepsilon^{2/3} k^{-5/3}$ , where  $C_k$  is the  
491 Kolmogorov constant ( $\sim 1.5$ ),  $\varepsilon$  is the turbulent kinetic energy dissipation rate and  $k$  is the wave-  
492 number ( $2\pi/\text{eddy diameter}$ ,  $\text{rad.m}^{-1}$ )<sup>46,47</sup>. Here we approximate this relationship as  $E(k) \propto$   
493  $k^{-5/3}$ , providing a dimension of  $\text{m}^{-1}$  (47). The spatial distribution of plankton has been  
494 observed to follow the same power law<sup>12,48</sup>, and the separation distance  $d$  as a function of size  
495 (both units in m) may therefore be considered as an implicit measure of the effect of dispersion  
496 due to turbulence. Thus, by considering  $d \propto k^{-5/3}$  we undertook a phenomenological correction  
497 for the abundances of nekton, whose foraging effort is impacted by the turbulent dispersal of  
498 plankton, by subtracting the Kolmogorov power law, intersecting at  $l = 0.1$  m, and calculated an  
499 adjusted scaling value for the entire data range.

## 500 **Rosenzweig-MacArthur model**

501 We used the classical Rosenzweig-MacArthur model to investigate the effect of turbulence on  
502 population dynamics and size-abundance relationships for consumer and resource pairs, from  
503 phytoplankton to whales. This formulation allows us to use previously defined allometric laws to  
504 generate a global size-abundance distribution. Despite the number of assumptions inherent in  
505 allometry, we note that macro-scale models parameterised by size have been found to outperform  
506 those which are defined based on species-specific traits and are also significantly more  
507 parsimonious<sup>49</sup>. To maintain consistency in units across empirical data, model, and adjustments,

508 size was given by (standardised) length in m and abundance was defined as organisms per meter  
509 ( $n \cdot m^{-1}$ ), i.e. the inverse of separation distance, rather than mass (kg) and biomass (density,  
510  $kg \cdot m^{-3}$ ). The base ordinary differential equation contains strictly positive parameters and is  
511 described by:

$$512 \quad \frac{\partial x}{\partial t} = rx \left(1 - \frac{x}{K}\right) - \frac{\varphi xy}{h + x}$$

$$513 \quad \frac{\partial y}{\partial t} = \frac{\varepsilon \varphi xy}{h + x} - \delta y$$

514 where  $x$  and  $y$  are resource and consumer (predator) abundances, respectively. The parameter  $h$   
515 denotes the half saturation, whereas  $K$  is the carrying capacity,  $r$  and  $\delta$  are birth and death rates,  
516  $\varepsilon$  the conversion efficiency, and  $\varphi$  the maximal consumption rate.

517

518 Each of the parameters follows scaling models according to the size ( $l$ , m) of the resource ( $l_x$ ) or  
519 consumer ( $l_y$ ), such that  $i = i_0 l^{\sigma_i}$ , for some parameter  $i$ , coefficient  $i_0$  and exponent  $\sigma_i$ . Scaling  
520 properties can change according to factors such as primary production rates, temperature, habitat  
521 complexity, among many others<sup>3</sup>. A constant temperature was assumed, and resource-consumer  
522 size ratios between 0.01 and 0.5 (corresponding to prey-predator mass ratios of 1E-6 and 0.1  
523 respectively), as scaling laws can change when the predator is smaller than the prey. Exponents  
524 were given by representative values from previous research, which was typically specialised on  
525 deriving empirical scaling for that specific parameter (Extended Data, Table S2). As our dataset  
526 ranges over more than 23 orders of mass magnitude, where there was some variability across  
527 literature scaling models, our study used the exponent values which were most consistent across  
528 the size range. Values chosen were (i) frequently reported with consensus ( $r, \delta, \varphi, K$ ), (ii) mid-



529 range ( $h$ ) or (iii) specifically calculated for aquatic vertebrates ( $\varphi_t$ ). Noting that rate-related  
530 parameters ( $r, \delta, \varphi_{v,t}$ ) will scale faster with length than mass, the scaling values are given as  
531 follows:  $r = r_0 l_x^{-0.75}$ ;  $K = K_0 l_x^{-0.75}$ ;  $h = h_0 l_y^{-0.75}$ ;  $\varphi_v = \frac{\varphi_{t0}}{\varepsilon_v} l_y^{-0.75}$ ;  $\delta = \delta_0 l_y^{-0.75}$ ;  $\varepsilon_v = \varepsilon_{v0} l_y^{1/8}$ .  
532 (Length scaling values of  $-3/4$  are equivalent to mass scaling values of  $-1/4$ .) We assumed  
533 carrying capacity scales according to  $-3/4$  as per null metabolic expectation, but note here that it  
534 does not impact equilibria values in the Rosenzweig-MacArthur system of ODEs (although it  
535 does affect behaviour of the limit cycle). The scaling values for two parameters change between  
536 the viscous and turbulent regime (organism length  $>0.1$  m):  $\varepsilon_t = \varepsilon_{t0} l_y^{-1.3}$  and  $\varphi_t = \frac{\varphi_{t0}}{\varepsilon_t} l_y^{-0.75}$ .  
537 Please refer to Extended Data, Table S2 for literature sources for exponents, and the biophysics  
538 section below for the derivations of  $\varepsilon$  scaling exponents. Under this parameterisation, there is a  
539 switch to a positive maximal consumption rate ( $\varphi$ ) in the turbulent regime. This has been  
540 previously noted in the functional response literature. Whilst invertebrates and microorganisms  
541 typically scale with a  $-0.75$  (length) exponent, which matches null model predictions derived  
542 under metabolic theory, data for macroscopic fauna in aquatic environments display positive  
543 scaling; our derived  $\approx 0.55$  exponent falls within observed empirical ranges<sup>11,49,50</sup>. Refer to  
544 Extended Data, Table S2 for more information.

545

546 The parameter scaling coefficients were standardised against phytoplankton/zooplankton models  
547 to ensure the boundary value for primary producers was feasible. The smallest primary producer  
548 (i.e.  $0.7 - 1 \mu\text{m}$  in length) was assumed to be the cyanobacterium *Prochlorococcus*<sup>51</sup>. For  
549 coefficients, biomass was divided by species mass to obtain the number of organisms. Model  
550 equilibria were calculated using analytical formulae solutions.

551

## 552 **Locomotion cost: biophysics derivations for the model**

553 To derive the biophysics portion of the model we integrate models across several disciplines. We  
554 use scaling of mass throughout this section to remain consistent with the literature, unless  
555 otherwise specified. To account for movement cost in the Rosenzweig-MacArthur system, we  
556 consider locomotion energy budgets across the whole size range (bacteria to whales). If  
557 movement energy usage scales equivalently to basal metabolic processes, its impacts would not  
558 be noticeable. However, if it scales differently, some of the energy previously used to create new  
559 biomass would instead be diverted to locomotion. Alternately, if locomotion were to become  
560 more efficient, additional energy could be provided for biomass. This can be seen by examining  
561 the gross metabolic power of an organism:

$$562 \quad P_{gross} = P_{basal} + P_{locomotion} \propto M^b + M^{loc}$$

563 Normalising by  $P_{basal}$  results in:

$$564 \quad \frac{P_{gross}}{P_{basal}} = 1 + \frac{P_{locomotion}}{P_{basal}} \propto 1 + M^{loc-b}$$

565 If there is a discrepancy between the power exponents, the (relative) locomotory power  
566 consumption will change across the size distribution.

567

568 This deviation can be captured within the parameter for biomass transfer efficiency  $\varepsilon$ . To achieve  
569 this, we use a classical ecological relation, which links basal and locomotory metabolic cost to  
570 abundance<sup>24,52</sup>:

$$571 \quad N \propto M^{-b-c+q(F-D)}$$

572 In this master equation,  $N$  is the population abundance, and  $c$  is the relative transport cost  
573 scaling. We have  $c := p - b$ , where  $b$  is basal metabolic scaling, and  $p$  is the scaling of transport  
574 cost ( $T_c$ ) defined below. The term  $q(F - D)$  describes search effort, including  $q$ , swim speed  
575 scaling, and the parameters  $F$  and  $D$ , which describe density/fragmentation and dimensionality of  
576 the resource space. Note that if the term  $-c + q(F - D)$  equates to zero, classical population  
577 dynamics apply. That is, the standard Rosenzweig-MacArthur system, with a typical value of  $\varepsilon$   
578 e.g. the prey-predator size ratio. However, when it is non-zero, it captures the shift in locomotion  
579 energy allocation across the size distribution. This provides the following relationship for  $\varepsilon$ :

580 
$$\varepsilon \propto M^{-c+q(F-D)}$$

581 In the subsequent derivations for the exponents of  $\varepsilon$ , we use empirical swim speed scaling results  
582 from Andersen *et al.*'s (2016) review of marine scaling laws: 1/4 and 1/6 for viscous and inertial  
583 swimmers respectively. This is important because it suggests the scaling of real-world nekton  
584 swimming speed is steeper than what would be theoretically derived for maximum efficiency.  
585 'Optimal' speed scaling would be given as 5/24 and 1/12 for viscous and inertial regimes  
586 (calculated according to methods in Bale *et al.* 2014 Supplementary Information, under the  
587 assumption of a 3/4 basal metabolic law).

588

589

590 *Search effort scaling ( $q(F - D)$ )*

591 The parameter  $q$  is the scaling of swimming speed. The dimensionality of the space,  $D$ , is taken  
592 as 3 for the turbulent regime. In the laminar/viscous regime, we consider  $D = D' = 2.4$ , to  
593 account for the patch constraint and the fact that organisms can use local information to optimise

594 their hunting strategies<sup>24</sup>. We set the fractal dimension of the space,  $F$ , to a mid-range value of  
595 1.9<sup>24</sup>.

596

597 *Transport cost scaling ( $p, c$ )*

598 In this section,  $\mu$  and  $\rho$  denote the viscosity and density of the liquid respectively. For the  
599 purposes of this study, we assume all physical fluid properties are constant as changes in  
600 transport cost due to pressure, salinity, or temperature fluctuations at depth or in tropical versus  
601 polar regions are negligible relative to the effect of changes in size of the organism.

602

603 Transport cost is defined as  $T_C = P/u$  where  $P$  is power and  $u$  is swimming speed<sup>9</sup>. The master  
604 equations for the power of swimmers in the viscous regime are given by  $P_{v.und} = \mu(fa)^2l$  for  
605 undulatory swimmers<sup>9</sup> and  $P_{v.pad} = 6\pi\mu\frac{1}{2}lu^2$  for paddlers<sup>53</sup>. Here,  $f$ ,  $a$  and  $l$  are the kick  
606 frequency, kick amplitude and body length respectively. By using the classical relationship  
607 determined by Bainbridge<sup>10,54</sup>

$$f \propto u/l \quad (2)$$

608 and assuming changes in the length measurements  $a, l$  are scaling approximately proportional to  
609  $M^{1/3}$ , we have  $P_{v.und} \propto M^{5/6}$  and  $P_{v.pad} \propto M^{5/6}$  after value substitutions. That is, the power  
610 cost scales equivalently for paddlers and undulatory swimmers in the viscous regime.

611

612 For the turbulent regime, the power of inertial swimmers is given by  $P_t = \rho(fa)^3A$ , where  $A$  is  
613 the frontal area of the organism (scaling as  $M^{2/3}$  accordingly)<sup>9,10</sup>. Once again, we use Equation 2

614 and substitute in mass scaling values to obtain  $P_t \propto M^{7/6}$ . Using the definition of transport cost,  
615 we obtain  $T_{C_v} \propto M^{7/12}$  for organisms in the viscous environment and  $T_{C_t} \propto M$  for the turbulent  
616 environment. As the units for  $T_C$  are J/m, it is possible to make it unitless via multiplying by  
617  $1/\rho v^2$ , which is a constant under our assumptions of fluid properties.

618 This means that:  $c_v = p_v - b = \frac{7}{12} - \frac{3}{4} = -\frac{1}{6}$ , and  $c_t = p_t - b = 1 - \frac{3}{4} = \frac{1}{4}$ .

619 With the values for  $c, q, F$  and  $D$ , we can now calculate the scaling for  $\varepsilon$  in the viscous and  
620 turbulent regime, which we then convert to length scaling:

$$621 \quad \varepsilon_v \propto M^{-c_v+q_v(F_v-D')} = M^{\frac{1}{6}+\frac{1}{4}\left(-\frac{1}{2}\right)} = M^{\frac{1}{24}}$$

$$622 \quad \propto l^{\frac{1}{8}}$$

$$623 \quad \varepsilon_t \propto M^{-c_t+q_t(F_t-D)} = M^{-\frac{1}{4}+\frac{1}{6}\left(-\frac{11}{10}\right)} = M^{-\frac{13}{30}}$$

$$624 \quad \propto l^{-1.3}$$

625 We switch between the parameterisations at the length of 0.1m, corresponding to the transition  
626 from laminar/mixed fluid regime to a fully turbulent flow of  $Re > 1000$ . Finally, normalising  
627 constants  $\varepsilon_{t_0}, \varepsilon_{v_0}$  set initial values. The resultant mean, maximum and minimum conversion  
628 efficiencies are 0.09, 0.2 and 4E-3 respectively, which are within expected literature values<sup>55</sup>.

629

### 630 **Fishing-induced evolution**

631 Fishing-induced evolution (FIE), specifically, quantifying phenotypic change, was assessed by  
632 extracting size/age at maturity data from 113 time series taken from 15 studies (Extended Data,  
633 Table S3). In some cases, this was provided as probability norms of weight or length at 50%  
634 maturity (Wp50 or Lp50). Time-series with large gaps or fewer than 20 measured time points  
635 were excluded. Data was manually extracted using WebPlotDigitizer (v 3.12) and visually

636 verified by replotting and super-positioning over the original. For plots without discrete data  
637 points (i.e. smooth line graphs), one data point per year was used. Each time series was  
638 normalised and then split in two halves, for which mean values were calculated for the  
639 first/second half of study period. This was imported into a data structure consisting of the mean  
640 values, data type (size or age at maturity, 50% maturity, Wp50 or Lp50), gender, species, and  
641 length of study. For testing the difference in means between the first and second halves of a  
642 study period, data was firstly assessed for normality by using a 2-sided Kolmogorov-Smirnov  
643 test (n=113, critical value=0.1262, observed values 0.0774 and 0.0958 for pre- and post-  
644 respectively, MATLAB R2016b, Mathworks). A paired t-test (SPSS 24.0.0.0, 2017) indicated a  
645 10.6% shift in mean value in the second half of the study period (df=112, 95% CI (9.4,11.9), 2-  
646 tailed, t-statistic -17.374, p<0.001).

647

648 **Methods References**

649

- 650 32 IMOS - Zooplankton Abundance (2020). Available from  
651 [http://www.marine.csiro.au/marq/edd\\_search.Browse\\_Citation?txtSession=9012](http://www.marine.csiro.au/marq/edd_search.Browse_Citation?txtSession=9012).  
652 Accessed 2020-04-10.
- 653 33 IMOS - Picoplankton flow cytometry (2020). Available from  
654 [http://www.marine.csiro.au/marq/edd\\_search.Browse\\_Citation?txtSession=14407](http://www.marine.csiro.au/marq/edd_search.Browse_Citation?txtSession=14407).  
655 Accessed 2020-04-10.
- 656 34 Ibarbalz, F. M. *et al.* Global trends in marine plankton diversity across kingdoms of life.  
657 *Cell* **179**, 1084-1097. e1021 (2019).
- 658 35 Righetti, D., Vogt, M., Zimmermann, N. E., Guiry, M. D. & Gruber, N. (PANGAEA,  
659 2019).
- 660 36 Righetti, D., Vogt, M., Zimmermann, N. E., Guiry, M. D. & Gruber, N. (2019).  
661 PHYTOBASE. Accessed 2020-04-15. doi: 10.1594/PANGAEA.904397.
- 662 37 Barneche, D., Kulbicki, M., Floeter, S. R., Friedlander, A. M. & Allen, A. Energetic and  
663 ecological constraints on population density of reef fishes. *Proceedings of the Royal*  
664 *Society B: Biological Sciences* **283**, 20152186 (2016).
- 665 38 WoRMS Editorial Board (2020). World Register of Marine Species. Available from  
666 <https://www.marinespecies.org> at VLIZ. Accessed 2020-05-10. doi:10.14284/170.
- 667 39 Forese, R. & Pauly, D. (2020). FishBase. Available from [www.fishbase.org](http://www.fishbase.org). Accessed  
668 2020-05-15.
- 669 40 Khachikyan, A. *et al.* Direct cell mass measurements expand the role of small  
670 microorganisms in nature. *Applied and environmental microbiology* **85** (2019).
- 671 41 Hatton, I. A. *et al.* The predator-prey power law: Biomass scaling across terrestrial and  
672 aquatic biomes. *Science* **349**, aac6284 (2015).
- 673 42 Hatton, I. A., Dobson, A. P., Storch, D., Galbraith, E. D. & Loreau, M. Linking scaling  
674 laws across eukaryotes. *Proceedings of the National Academy of Sciences* **116**, 21616-  
675 21622 (2019).
- 676 43 Politis, D. N., Romano, J. P. & Wolf, M. *Subsampling*. (Springer Science & Business  
677 Media, 1999).
- 678 44 Romano, J. P. & Wolf, M. Subsampling intervals in autoregressive models with linear  
679 time trend. *Econometrica* **69**, 1283-1314 (2001).
- 680 45 Williams, I. D. *et al.* Human, oceanographic and habitat drivers of central and western  
681 Pacific coral reef fish assemblages. *PLoS One* **10** (2015).
- 682 46 Kolmogorov, A. N. The local structure of turbulence in incompressible viscous fluid for  
683 very large Reynolds numbers. *Dokl. Akad. Nauk SSSR* **30**, 299-303.
- 684 47 Tennekes, H. & Lumley, J. L. *A first course in turbulence*. (MIT press, 2018).
- 685 48 Yamazaki, H., Mitchell, J. G., Seuront, L., Wolk, F. & Li, H. Phytoplankton  
686 microstructure in fully developed oceanic turbulence. *Geophysical research letters* **33**  
687 (2006).
- 688 49 Kalinkat, G. *et al.* Body masses, functional responses and predator-prey stability.  
689 *Ecology letters* **16**, 1126-1134 (2013).
- 690 50 Rall, B. C. *et al.* Universal temperature and body-mass scaling of feeding rates. *Phil.*  
691 *Trans. R. Soc. B* **367**, 2923-2934 (2012).

- 692 51 Partensky, F., Hess, W. R. & Vaulot, D. Prochlorococcus, a marine photosynthetic  
693 prokaryote of global significance. *Microbiology and molecular biology reviews* **63**, 106-  
694 127 (1999).
- 695 52 Haskell, J. P., Ritchie, M. E. & Olf, H. Fractal geometry predicts varying body size  
696 scaling relationships for mammal and bird home ranges. *Nature* **418**, 527 (2002).
- 697 53 Mitchell, J. G. The energetics and scaling of search strategies in bacteria. *The American*  
698 *Naturalist* **160**, 727-740 (2002).
- 699 54 Bainbridge, R. The speed of swimming of fish as related to size and to the frequency and  
700 amplitude of the tail beat. *Journal of experimental biology* **35**, 109-133 (1958).
- 701 55 Parsons, T. R. & Chen, Y.-L. L. Estimates of trophic efficiency, based on the size  
702 distribution of phytoplankton and fish in different environments. *Zool. Stud* **33**, 296-301  
703 (1994).
- 704

705